Available online at www.sciencedirect.com
ScienceDirect
Inorganica Chimica Acta xxx (2007) xxx–xxx
Inorganica Chimica Acta
www.elsevier.com/locate/ica

A seven-coordinate Fe^{III} compound: $[Fe\{O(CH_2CO_2)_2\}(H_2O)_2(NO_3)]$. Preparation, structure and magnetic properties

Leonardo D. Slep [a], Rafael Calvo [b,*], Otaciro R. Nascimento [c], Ricardo Baggio [d], María T. Garland [e], Octavio Peña [f], Mireille Perec [a,*]

[a] *Departamento de Química Inorgánica, Analítica y Química Física, Facultad de Ciencias Exactas y Naturales, INQUIMAE, Universidad de Buenos Aires, Ciudad Universitaria, Pabellón II, 1428 Buenos Aires, Argentina*
[b] *Departamento de Física, Facultad de Bioquímica y Ciencias Biológicas, Universidad Nacional del Litoral, and INTEC (CONICET-UNL), Güemes 3450, 3000 Santa Fe, Argentina*
[c] *Grupo de Biofísica Molecular Sergio Mascarenhas, Departamento de Física e Informática, Instituto de Física de São Carlos, Universidade de São Paulo, C.P. 369, CEP 13560-970, São Carlos, SP, Brazil*
[d] *Departamento de Física, Comisión Nacional de Energía Atómica, Av. Gral. Paz 1499, 1650 San Martín, Buenos Aires, Argentina*
[e] *Departamento de Física, Facultad de Ciencias Físicas y Matemáticas, Universidad de Chile, Av. Blanco Encalada 2008, Casilla 483, Santiago, Chile*
[f] *UMR 6226 CNRS, Sciences Chimiques de Rennes, Université de Rennes 1, 35042 Rennes, France*

Received 29 December 2006; accepted 10 February 2007

Abstract

A seven-coordinate Fe^{III} complex, $[Fe(oda)(H_2O)_2(NO_3)]$, was obtained after dissolving $Fe(NO_3)_3 \cdot 9H_2O$ in an aqueous solution of oxydiacetic acid (H_2oda) at room temperature. In the solid state, the Fe^{III} center adopts a pentagonal bipyramid geometry with an $\{FeO_7\}$ core formed by a tridentate oda^{2-} and a bidentate NO_3^- in the equatorial plane, and two axial water molecules. Magnetic measurements and EPR spectra revealed the presence of $S = 5/2$ Fe^{III} centers with rhombic zero field splitting parameters ($D = 0.81\ cm^{-1}$, $E/D = 0.33$). Weak antiferromagnetic interactions with $J \approx -0.06\ cm^{-1}$ operating between neighboring Fe ions connected through Fe–O–C–O···H–O–Fe paths are estimated using the molecular field approximation.

Keywords: Fe^{III}; Oxydiacetato; X-ray crystal structure; Magnetic properties; EPR

1. Introduction

The hydrolytic chemistry of Fe^{III} has been extensively studied due to its importance in natural iron mineralization processes, which lead to the formation of thermodynamically stable polyiron oxo/hydroxo compounds containing the Fe–$(O)_n$–Fe/Fe–$(OH)_n$–Fe motifs [1–4]. Strong chelating ligands can diminish or even suppress these processes in aqueous media, offering the opportunity of trapping oligomeric or even mononuclear species [5]. These processes become particularly significant in living systems, where iron is acquired, transported and stored mostly by low-molecular-weight compounds involving multidentate oxygen donors from carboxylate, hydroxamate and catecholate ligands [6,7].

Studies of the products generated by controlled hydrolysis of Fe^{III} in the presence of oxygen donors that mimic the natural ones are relevant not only to understand transport and storage of iron in living systems, but also as structural and spectroscopic models for some non-heme iron metalloprotein-active centers. Among the family of multidentate oxygen donor species, the 2,2′-oxydiacetato ligand

* Corresponding authors.
E-mail addresses: calvo@fbcb.unl.edu.ar (R. Calvo), perec@qi.fcen.uba.ar (M. Perec).

0020-1693/$ - see front matter © 2007 Elsevier B.V. All rights reserved.
doi:10.1016/j.ica.2007.02.031

(oda = $[O(CH_2CO_2^-)_2]$) stands as a versatile complexing agent. It holds five oxygen donor atoms and can complex metal ions by forming up to five-membered chelate rings. This ligand has been extensively used with magnetic and nonmagnetic metals of variable charge and coordination numbers; a wide variety of structures containing this anion in different environments are found in the Cambridge Structural Database System [8]. A linear polymeric Fe(II)-oda complex with concatenated $\{Fe(oda)(H_2O)_2$ units has been lately reported [9]. Concerning Fe^{III} compounds, the crystal structures of only two six-coordinate mononuclear and isostructural complexes of formula $[Fe(oda)(H_2O)_2X]$ (X = Cl, Br) have been reported. A nitrate complex ($X = NO_3^-$) was prepared but could not be crystallized [10].

There are about one hundred different seven-coordinate Fe^{III} complexes on the Cambridge Crystallographic Database [8], however complexes containing the $\{Fe^{III}O_7\}$ core are quite rare, to our knowledge it has only been reported for a macrocyclic calixarene Fe^{III} derivative acting as a cation receptor [11], in the core of a mixed-valent polynuclear oxo complex that models the biomineralization of the ferritin [12] and in tris(nitrato)(triphenylphosphine oxide)Fe^{III} [13].

Herein, we report the crystal structure, magnetic properties and EPR spectrum of $[Fe(oda)(H_2O)_2(NO_3)]$, (**1**), in which the iron atom is connected to a tridentate oda and a bidentate nitrate forming a nearly regular pentagon in the equatorial plane, and to two short axial water molecules. This unusual structure with a $\{Fe^{III}O_7\}$ core provides an interesting model compound for precursors of oxo/hydroxo reactions and provides insight into how the active sites of enzymes may change upon substrate and/or cofactor binding.

2. Experimental

2.1. Preparation and characterization

All chemicals employed were of reagent grade and used without further purification. Water was purified by a Millipore milli-Q system yielding 18 MΩ cm water. CHN elemental analyses were performed on a Carlo Erba 1108 elemental analyzer. Infrared spectra were recorded as KBr pellets and as Nujol mulls on a Nicolet 510P FT-IR spectrophotometer. Thermogravimetric measurements were carried out using a Shimadzu DTG 50 thermal analyzer under an air flow of 40 L/min at a heating rate of 5 °C min^{-1}.

An aqueous solution, 50 mL, of oxydiacetic acid (0.200 g, 3 mmol) was added to solid $Fe(NO_3)_3 \cdot 9H_2O$ (0.40 g, 3 mmol) under stirring at room temperature. Orange-brown crystals of the complex began to form immediately. The product was filtered off, washed with iced water and dried in air. Yield: 0.180 g, 60%. Calc. for $C_4H_8NO_{10}Fe$: C, 16.80; H, 2.80; N, 4.90. Found: C, 16.65; H, 2.85; N, 4.70%. FT-IR (KBr disc ν/cm^{-1}): 2940vs, vbr, 1564vs, vbr $(CO_2)_{asym}$, 1465s, 1423s $(CO_2)_{sym}$, 1384s, 1349s, 1310s, 1276vs $(NO_2)_{asym}$, 1236s, 1109s (C–O–C), 1027vs $(NO_2)_{sym}$, 947s, 857m, 804s, 773vs, 737s 593m, 498m. The isolated crystals can, however, be kept in dry air for several months and TGA analysis shows that they are thermally stable up to 200 °C, whereupon degradation occurs in overlapping steps involving the simultaneous loss of coordinated water and skeleton collapse, leading to the final residue Fe_2O_3 at 300 °C.

2.2. Structural determination

X-ray quality single crystals were glued on the tip of glass fibers and data were collected at room temperature (298(2) K) on a Bruker SMART CCD diffractometer, with graphite monochromated Mo Kα radiation (λ = 0.71069 Å). The structure was primarily solved by direct methods and completed by difference Fourier synthesis. Refinement of the model was performed by full-matrix least-squares techniques with anisotropic thermal factors for all non-H atoms. Theoretical models fixed the hydrogen atoms of the compound. All calculations were performed using the program package SHELXL-97 [14]. Full use of the CCDC package was made using the CSD Database [8]. A summary of the crystallographic data and details of the structure refinement are given in Table 1.

2.3. Magnetic and EPR measurements

Susceptibility and magnetization measurements were performed on finely powdered samples with a Quantum Design Squid magnetometer model MPMS XL5, using calibrated gelatin capsules as sample holders having small diamagnetic contribution. The magnetic susceptibility was measured in the temperature interval 2–300 K, with an applied field of 25 mT. The magnetization measurements were performed at 2 and 5 K, with a maximum field of 5 T. The contribution of the gelatin capsule was subtracted from the measured values. The diamagnetic correction per mol of iron was estimated from Pascal's constants [15–17] as $\chi_{dia} = -130 \times 10^{-6}$ cm^3 mol^{-1}. A temperature indepen-

Table 1
Crystal data and structure refinement for $[Fe(oda)(H_2O)_2(NO_3)]$

Empirical formula	$C_4H_8FeNO_{10}$
Formula weight	285.96
Temperature (K)	298
Crystal system	orthorhombic
Space group	*Aba2* (No. 41)
Unit cell dimensions	
a (Å)	9.2473(16)
b (Å)	10.3115(18)
c (Å)	9.3771(17)
Volume (Å^3)	894.1(3)
Z	4
D_{calc} (g/cm^3)	2.124
Absorption coefficient μ(Mo Kα) (mm^{-1})	1.74
Reflections collected/unique	3382/985
$R_{int}/wR(F^2)$	0.023, 0.069 (all data)

CCDC Reference Number 623026.

dent paramagnetic contribution $\chi_{TIP} = 331 \times 10^{-6}$ emu mol^{-1} was estimated from the high temperature behavior of the observed $\chi(T)T$ versus T curve.

The electron paramagnetic resonance (EPR) spectra of a fine powdered sample of **1** were recorded as a function of temperature between 4 and 77 K with a Bruker ELEXSYS E580 spectrometer (Bruker BioSpin, Germany) working at 9.48 GHz. The temperature was controlled by an Oxford ITC503 cryogenic system.

2.4. Computational details

All calculations were performed with the program package ORCA [18] at the B3LYP level of DFT [19,20]. We employed the all-electron Gaussian basis sets reported by the Ahlrichs group [21,22]. The whole set of atoms was described by triple-ζ valence basis sets with one set of polarization (TZV(P)) functions [22]. The auxiliary basis sets used to fit the electron density were taken from the Turbomole library [23] and were chosen to match the orbital basis. The SCF calculations were of the spin-polarized type and were tightly converged (10^{-7} Eh in energy, 10^{-6} in the density change and 10^{-6} in maximum element of the DIIS [24] error vector).

3. Results and discussion

3.1. Synthesis and solid state structure

Crystallographic data are given in Table 1, and relevant distances and angles in Tables 2a and 2b. The structure consists of discrete [Fe(oda)$(H_2O)_2(NO_3)$] units, with seven-coordinate Fe^{III} centers showing pentagonal bipyramidal geometry (Fig. 1). The whole assembly is bisected by a twofold axis passing through the cation, the ether oxygen O3 in oda, the nitrate nitrogen N and O5, thus rendering only half of the molecule independent.

The five-coordinate positions in the equatorial plane are occupied by three oxygen atoms of the tridentate oda and two oxygens from a bidentate nitrate, with a mean deviation from planarity of 0.0439(1) Å. This is consistent with the IR data which show vibrational bands at 1564, 1423 and 1109 and at 1276 and 1027 cm^{-1}, respectively, which are characteristics of oda tridentate *mer* conformation and of a chelating nitrate group [25,26].

The axial positions are occupied by two strongly bonded aqua molecules at distances of 2.0045(18) Å subtending an aq–Fe–aq interaxial angle of 174.09(15)°, and 3.42(17)° to the vertical plane. The two symmetry related halves of the oda ligand do not form a strict plane as the calculation of the mean plane through the Fe–O3 symmetry axis reveals; the main (symmetric) departures are for atom pairs O1, O1^{i} and C2, C2^{i} with deviations of 0.093 and 0.070 Å, respectively, at both sides of the plane. The ligands present well differentiated coordination strengths, with the Fe–O bond lengths decreasing in the order aqua < oda < NO_3. Their structures are normal: the oda carboxylates present almost identical C–O bond lengths, while the nitrate unit shows clearly its bidentate coordination with N–O_{coord} being some 5.5% longer than N–$O_{uncoord}$ and the bite angle 6% smaller than the other two angles, symmetrically equivalent. The aqua hydrogens are involved in strong H-bonds (Tables 2a and 2b), which is due to the different orientations adopted by the molecules in the unit cell which end up configuring a tightly woven 3D network that stabilizes the structure (Fig. 2).

3.2. Magnetic and EPR results

The temperature dependence of the magnetic susceptibility was measured for [Fe(oda)$(H_2O)_2(NO_3)$] in the

Table 2a
Selected bond lengths (Å) and angles (°) for [Fe(oda)$(H_2O)_2(NO_3)$] (**1**)

Fe–O1W (×2)	2.0045(18)	Fe–O3	2.101(4)
Fe–O1 (×2)	2.0288(18)	Fe–O4 (×2)	2.160(2)
O1–C1	1.257(3)	O3–C2	1.422(3)
O2–C1	1.251(3)	C1–C2	1.506(4)
O4–N	1.272(3)	O5–N	1.205(6)
O1W–Fe–O1W^{i}	174.09(15)	O1–Fe–O4	76.81(8)
O1^{i}–Fe1–O3	73.67(6)	O4–Fe1–O4^{i}	59.22(10)
O5–N–O4	122.9(2)	O4–N–O4^{i}	114.2(4)

Symmetry code: ^{i} $-x+2, -y, z$.

Table 2b
Hydrogen bonds for [Fe(oda)$(H_2O)_2(NO_3)$] (**1**) (Å and °)

D–H···A	*d*(D–H) (Å)	*d*(H···A) (Å)	*d*(D···A) (Å)	∠(DHA) (°)
O1W^{ii}–H1WA^{ii}···O2	0.85(2)	1.850(13)	2.678(3)	165(4)
O1W^{iii}–H1WB^{iii}···O2	0.85(2)	1.870(14)	2.700(3)	165(4)

Symmetry codes: ^{ii} $x, y+1/2, z+1/2$; ^{iii} $-x+3/2, y+1/2, z$.

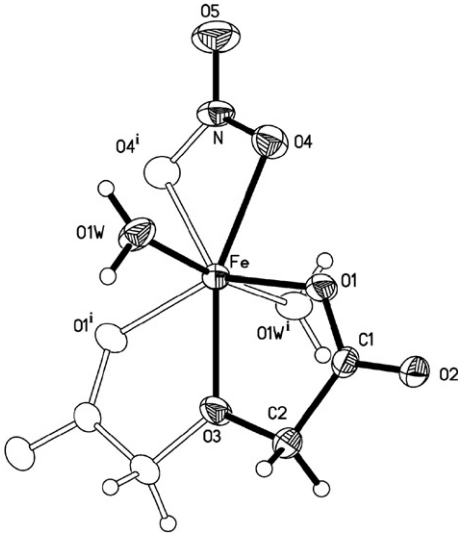

Fig. 1. Perspective view of [Fe(oda)$(H_2O)_2(NO_3)$] (**1**) with thermal ellipsoids at the 50% probability level. Symmetry codes as in Table 1.

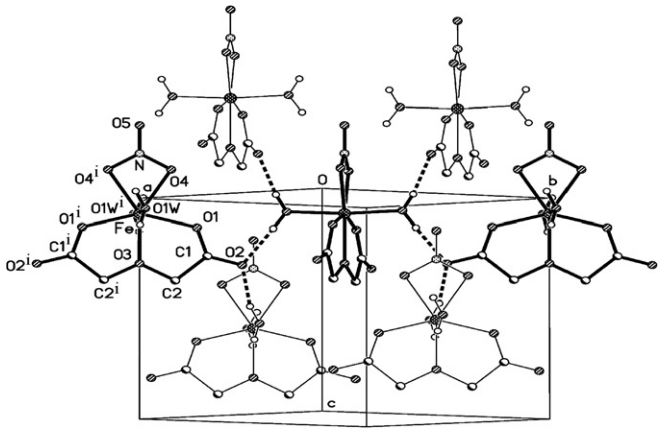

Fig. 2. Packing diagram for $[Fe(oda)(H_2O)_2(NO_3)]$ (**1**), showing the H-bonding. Symmetry codes as in Table 1.

temperature range 2–300 K. The data show the characteristic features of a paramagnetic compound as indicated by the $\chi_m T$ product versus T plot depicted in Fig. 3a. At room temperature, $\chi_m T = 4.37$ emu K mol^{-1} is close to the expected value for an isolated Fe^{III} ion with $S = 5/2$, as expected for high spin five unpaired electrons. $\chi_m T$ decreases at lower temperatures, to reach a value of 1.10 emu K mol^{-1} at 2 K. The isothermal magnetization curves at 2 and 5 K show that the saturation value of 5 μ_B expected for an $S = 5/2$ ion is not reached at the highest field, 5 T (Fig. 3b). The spin Hamiltonian describing the magnetic behavior of **1** is written as

$$\mathscr{H} = \sum_i [\mathscr{H}_z(i) + \mathscr{H}_{zfs}(i)] + \sum_{i \neq j} [\mathscr{H}_{ex}(i,j) + \mathscr{H}_{dip}(i,j)] \quad (1)$$

where $\mathscr{H}_z(i)$ and $\mathscr{H}_{zfs}(i)$ are the "single ion" Zeeman and zfs interactions acting on spin i. In the coordinate system where the zfs is diagonal, and considering an isotropic g-tensor, they can be written as

$$\mathscr{H}(i) = g\mu_B \mathbf{S}_i \cdot \mathbf{H} + D\left[S_{iz}^2 - \frac{S(S+1)}{3}\right] + E[S_{ix}^2 - S_{iy}^2] \quad (2)$$

where $\mathbf{S}_i$ is the spin operator of the Fe^{III} ion in site i, μ_B the Bohr magneton, $\mathbf{H}$ the applied magnetic field and D and E the zfs parameters. $\mathscr{H}_{zfs}$ has the point symmetry of the Fe^{III} site and one of their principal directions is along the c crystal axis (see Fig. 2). $\mathscr{H}_{ex}(i,j)$ and $\mathscr{H}_{dip}(i,j)$ are the exchange and dipolar couplings between Fe ions in sites i and j. $\mathscr{H}_{ex}(i,j)$ can be written as [17]

$$\mathscr{H}_{ex}(i,j) = -J_{ij}\mathbf{S_i} \cdot \mathbf{S_j} \quad (3)$$

where the isotropic exchange coupling parameter J_{ij} is related to the chemical paths connecting he metal ions [17]. The anisotropic dipole–dipole interactions, $\mathscr{H}_{dip}$ [16], are transmitted through space and their contribution to the susceptibility and magnetization is averaged out when measured in powder samples. Meanwhile, when the g-value is nearly isotropic, the zero field splitting and dipolar terms are the most important for the EPR spectrum. We modeled the susceptibility and magnetization considering Fe ions with a zero field splitting (Eq. (1)), exchange coupled (Eq. (3)) to z identical Fe neighbors. These exchange couplings were considered within the molecular field approximation [17,27]. Best fit parameters obtained with a least-squares analysis of the temperature dependence of the experimental values of $\chi(T)T$ versus T shown in Fig. 3a and the magnetization isotherms shown in Fig. 3b are $g = 1.965$, $D = 0.81$ cm^{-1}, $E/D = 0.33$, $zJ = -0.24$ cm^{-1}. Fig. 3a and b display the satisfactory match obtained between the magnetic data and the curves calculated with these values. The g value obtained in the fitting is smaller than the free electron value, a fact that we attribute to the presence of excess water in the sample. Absorption of diamagnetic water by the solid would lead to slight errors in the molecular-weight and diamagnetic corrections used, both of which would affect the g value derived from magnetic susceptibility in the observed direction. Nevertheless, this problem does not affect the quality of the obtained zfs parameters. The negative value of zJ indicates a rather small effective antiferromagnetic interaction among Fe^{III} centers.

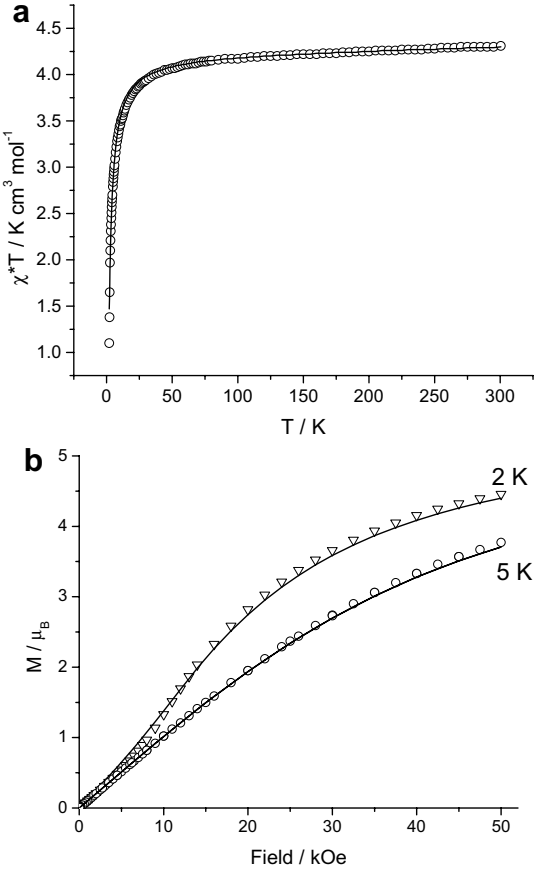

Fig. 3. (a) Temperature variation of the χ_mT product. (b) Magnetic field dependence of the molar magnetization at 2 and 5 K. The solid lines correspond to the best fit according to the spin-Hamiltonian described in the text.

To analyze the origin and magnitudes of the Fe–Fe interactions, we turn back to the X-ray structure, which

shows that each metal center is surrounded by 12 homologous nearest neighbors conforming a fcc lattice with a mean Fe···Fe distance of 6.78 Å. This arrangement is important for the magnetic dipolar interactions $\mathscr{H}_{dip}$ that are transmitted through space and are proportional to S^2 and thus relatively large for **1**. Meanwhile, as shown in Fig. 4, the through-bond connectivities giving rise to exchange interactions between neighbor Fe centers (Eq. (3)) are achieved via three different types of pathways involving carboxylate groups and H-bonds (see Fig. 4). The chemical paths (a) and (b) are nearly equivalent (Fe–Fe distances 9.212 and 9.237 Å) and involve one H-bond and a carboxylate bond. Path (c) is somewhat longer (9.427 Å) and involves two H-bonds. Since the covalent carboxylate bond is more efficient to transmit exchange interactions than the H-bond, the contribution of path (c) is expected to be significantly weaker and may be neglected. Each Fe ion is connected to two Fe neighbors through path (a) and to two other Fe neighbors through path (b). If paths (a) and (b) are considered equivalent (see Tables 2a and 2b), $Z = 4$ and $J \approx -0.06\ cm^{-1}$ in the molecular field approximation. This equivalence is not exactly valid because the bond angles in the path are different but it is a reasonable approximation considering that for long paths the details of the bonds are less important compared with the nature of each section of the path (covalent section, H-bond, etc.) [28].

The EPR spectrum of **1** observed at 7.5 K is displayed in Fig. 5. It is a broad resonance with a peak to peak width of ~500 mT with no structure and little information. No major variation of the spectrum, except some broadening, is observed up to temperatures of 77 K, when the resonance starts to disappear. It was simulated using EasySpin [29] considering the values of the zfs parameters calculated from the magnetic results but neglecting dipolar interactions between Fe ions. The result has much narrower linewidths than the experimental results. As described by Pilbrow [30], the zero field splitting is larger than the microwave energy ($D > g\mu_B H$) and in the extreme rhombic limit ($E/D \sim 1/3$), as indicated by the magnetic data, the simulated spectrum of a powder sample displays a strong peak at $g \sim 4.3$ and a broad peak spread over a large range of low g-values. Our simulations reflect this behaviour, but the observed width of the broad peaks cannot be explained assuming random distributions of the zero field splittings. We attribute the broadening to dipolar interactions between a Fe ion and its Fe neighbors in the approximate fcc lattice. The magnitude of the dipolar field produced by an Fe ion at a neighboring Fe at 6.78 Å is about 50 mT. The magnitude of the dipolar coupling decreases with the cube of the distance and the number of neighbors increases with the square of the distance; thus the dipolar interaction decreases only linearly with distance and many spheres of neighbors should be considered, making a simulation unmanageable. We concluded that the observed width of the resonance is very likely produced by the random dipolar interactions between an Fe ion and the rest of the fcc lattice. However, since it is not possible to simulate such EPR spectrum, only a qualitative explanation can be given.

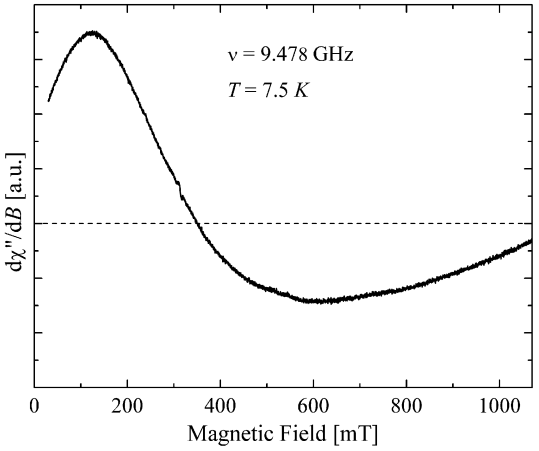

Fig. 5. X-band EPR spectrum of a powdered sample of [Fe(oda)$(H_2O)_2(NO_3)$] (**1**) at 7.5 K. Experimental conditions: microwave frequency 9.478 GHz, modulation amplitude, 1 Oe; modulation frequency, 100 kHz; microwave power, 10 mW.

A single-point DFT-based computation [31,32] performed on an isolated molecule at the experimental seven-coordinate geometry yields an almost isotropic g-matrix with principal values 2.005, 2.008 and 2.014, which results in a $g_{iso} = 2.012$, not far from the free electron value of 2.0023. The spin–orbit coupling contribution to the zero field splitting tensor accounts for a D value of 0.53 cm^{-1} and $E/D = 0.28$, in good agreement with the experimental values.

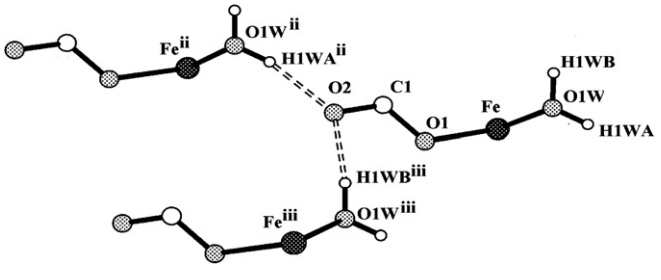

Fig. 4. The three independent Fe···Fe interaction paths showing Fe···Fe distances (d) and path-lengths measured along the bonds (d′) in the lattice: (a) Fe–O1–C1–O2···[H1WA–O1W–Fe]^{ii} with d = 6.969 Å and d′ = 9.212 Å; (b) Fe1–O1A–C1A–O2A···[H1WB–O1W–Fe1]^{iii} with d = 6.925 Å and d′ = 9.237 Å (c) [Fe1–O1W–H1WA]^{ii}···O2A···[H1WB–O1W–Fe1]^{iii} with d = 6.585 Å and d′ = 9.427 Å. Symmetry codes as in Tables 2a and 2b.

4. Conclusions

A 3D structure with mononuclear {Fe^{III}–O_7} cores was obtained by reacting oxydiacetic acid with $Fe(NO_3)_3 \cdot 9H_2O$ in water at room temperature. The crystallization of seven-coordinate [Fe(oda)$(H_2O)_2(NO_3)$] from a solution likely to contain a variety of species depends, we believe, upon the stabilizing effect of H-bond interactions. A key

feature in the stabilization appears to be the rigidity of the oda ligand promoting intermolecular H-bonds with the axial aqua water molecules. The magnetic measurements allowed to determine the zero field parameters of the Fe^{III} ions with $S = 5/2$, and show weak antiferromagnetic couplings between Fe^{III} neighbors transmitted through paths containing an H-bond and a carboxylate bond.

Acknowledgements

We thank the Spanish Research Council (CSIC) for providing some of us with free-of-charge licenses to the Cambridge Structural Database. The work in Argentina was supported by grants PIP 5274, CAI+D-UNL and ANPCyT PICT 06-13782. Work in Chile was supported by grant CONICYT-FONDAP 11980002. We acknowledge the binational grant ECOS-Sud Francia-Argentina A05E01. LS, RC and MP are members of CONICET.

References

[1] K.S. Hagen, Angew. Chem. 104 (1992) 1036.
[2] K.S. Hagen, Angew. Chem. Int. Ed. Engl. 31 (1992) 1010.
[3] D.M. Kurtz Jr., Chem. Rev. 90 (1990) 585.
[4] V.L. Pecoraro, M.J. Baldwin, A. Gelasco, Chem. Rev. 94 (1994) 807.
[5] C.J. Harding, R.K. Henderson, A.K. Powell, Angew. Chem., Int. Ed. Engl. 32 (1993) 570.
[6] M. Costas, M.P. Mehn, M.P. Jensen, L. Que, Chem. Rev. 104 (2004) 939, and references cited therein.
[7] S.J. Lippard, Principles of Bioinorganic Chemistry, University Science Books, Mill Valley, CA, 1994.
[8] F.H. Allen, Acta Crystallograllogr., Sect. B 58 (2002) 380.
[9] A. Grirrane, A. Pastor, C. Mealli, A. Ienco, P. Rosa, R. Prado-Gator, A. Galindo, Inorg. Chim. Acta 357 (2004) 4215.
[10] A.K. Powell, J.M. Charnock, A.C. Flood, C.D. Garner, M.J. Ware, W. Clegg, J. Chem. Soc., Dalton Trans. (1992) 203.
[11] M.I. Ogden, B.W. Skelton, A.H. White, J. Chem. Soc., Dalton Trans. (2001) 3073.
[12] K.L. Taft, G.C. Papaefthimiou, S.J. Lippard, Science 259 (1993) 1302.
[13] A.N. Chekhlov, Russ. J. Inorg. Chem. 50 (2005) 1303.
[14] G.M. Sheldrick, SHEXTL 97, Programs for solution and refinement of crystal structures, University of Göttingen, Göttingen, Germany, 1997.
[15] P. Pascal, Ann. Chim. Phys. 19 (1910) 5.
[16] R. Carlin, Magnetochemistry, Springer, Berlin, 1986.
[17] O. Kahn, Molecular Magnetisn, Wiley VCH, New York, 1993.
[18] ORCA – an Ab Initio, Density functional and Semiempirical Program Package 2.4, Max-Planck Institut für Bioanorganische Chemie, Mülheim an der Ruhr, Germany, 2004.
[19] J.P. Perdew, Phys. Rev. B 33 (1986) 8822.
[20] A.D. Becke, J. Chem. Phys. 84 (1988) 4524.
[21] A. Schäfer, H. Horn, R. Ahlrichs, J. Chem. Phys. 97 (1992) 2571.
[22] A. Schäfer, C. Huber, R. Ahlrichs, J. Chem. Phys. 100 (1994) 5829.
[23] Basis sets can be obtained form the ftp server of the Turbomole homepage at http://www.turbomole.com.
[24] P. Pulay, Chem. Phys. Lett. 73 (1980) 393.
[25] K. Nakamoto, Infrared and Raman Spectra of Inorganic and Coordination Compounds, Part 3, fourth ed., John Wiley and Sons, New York, 1986.
[26] A. Grirrane, A. Pastor, A. Ienco, C. Mealli, A. Galindo, J. Chem. Soc., Dalton Trans. (2002) 3771.
[27] C.J. O'Connor, Prog. Inorg. Chem. 29 (1982) 203.
[28] R. Calvo, App. Magn. Resonan, in press.
[29] S. Stoll, A. Schweiger, J. Magn. Reson. 178 (2006) 42.
[30] J.R. Pilbrow, Transition Ion Electron Paramagnetic Resonance, Clarendon Press, Oxford, 1990.
[31] F.J. Neese, Chem. Phys. 115 (2001) 11080.
[32] D. Ganyushin, F. Neese, J. Chem. Phys. 125 (2006) 024103.